ChemComm

Check for updates

Photoinduced electron transfer from the naphthalene diimide anion radical doublet excited state†

Soojin Kim,[a] Charles J. Zeman IV,[ab] Habtom B. Gobeze,[a] Naresh Duvva[a] and Kirk S. Schanze ✱[a]

The dynamics of bimolecular photoinduced electron transfer from the doublet excited state of the anion radical of N,N′-dioctylnaphthalene diimide (NDI) have been investigated using picosecond transient absorption and fluorescence lifetime decay analysis. Stern–Volmer quenching studies afford the bimolecular quenching rate constants (k_q) for 18 acceptors.

Chart 1

Anion radical doublet excited states are currently attracting significant interest in the fields of photochemistry and electron transfer (ET) photocatalysis.[1–4] The interest is motivated by the understanding that the excited states of anion radicals can serve as potent one-electron reductants.[3,5,6] Since anion radicals can be produced by photoreduction in the presence of a sacrificial reducing agent, consecutive photoinduced electron transfer (conPET) to first generate the anion radical, followed by excitation of the radical ion to produce the doublet excited state, can lead to very effective photocatalysts to drive reactions that are triggered by reduction.[7] Consecutive photoinduced ET has recently gained interest as a tool in organic synthesis, leading to the development of synthetically useful examples.[8]

While several synthetic photocatalysis applications of con-PET have been developed, mechanistic study of the photophysics and ET reactivity of anion radical doublet excited states has lagged.[9] Several groups have explored the photophysics of anion radical excited states, including Wasielewski, Majima, Vauthey, and others.[3,10–23] We recently reported a study that used picosecond transient absorption (TA) spectroscopy to study bimolecular ET quenching of the anion radical excited state of perylene diimide (*PDI⁻•).[24] The study demonstrated that the ET quenching kinetics followed a Rehm–Weller correlation[25] of electron transfer quenching rate with the reduction potential of the quenchers. The
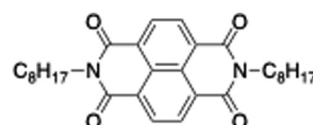
Rehm–Weller correlation was consistent with an excited state oxidation potential, $E(*\text{PDI}^-•/\text{PDI})$ of −1.87 V (all potentials are *vs.* SCE), and the TA study provided evidence for the products of the PET reaction with strong electron acceptors.[24]

N,N′-Dioctylnaphthalene diimide (NDI, Chart 1) is another member of the Rylene diimide family[26] that features a stable anion radical that absorbs strongly in the visible region.[10] The first reduction potential of the neutral diimide, $E(\text{NDI}/\text{NDI}^-•)$, is −0.56 V, and previous studies have shown that the doublet excited state can be detected by picosecond TA spectroscopy and has a lifetime of ∼200 ps.[10] In this communication we describe an investigation of bimolecular photoinduced ET reactions of the doublet excited state of the NDI anion radical, *NDI⁻•. We utilized picosecond TA and time resolved emission lifetime spectroscopy to carry out Stern–Volmer quenching studies with a series of electron acceptors with a wide range of reduction potentials. Rehm–Weller analysis of the quenching kinetics is consistent with an excited state oxidation potential for the doublet excited state anion radical, $E(*\text{NDI}^-•/\text{NDI}) = −2.1$ V. Remarkably, TA spectroscopy provides clear evidence for cage escape following the bimolecular electron ET reactions,[27] and the cage escape efficiency correlates with the reduction potential of the acceptor in a meaningful way. Analysis indicates for the systems with highest cage escape efficiency, the forward photoinduced ET reaction occurs in the Marcus inverted rection, whereas the return ET reaction that competes with cage escape is in the Marcus normal region.[28] This very unusual behavior occurs because *NDI⁻• is a very strong photoreductant.

For the work reported herein, solutions of the anion radical of N,N-dioctylnaphthalene diimide (NDI•⁻) were generated by

[a] *Department of Chemistry, University of Texas at San Antonio, One UTSA Circle, San Antonio, TX. 78249, USA. E-mail: kirk.schanze@utsa.edu*

[b] *Department of Chemistry, University of Florida, Gainesville, FL 32611, USA*

thermal reduction in an inert atmosphere glovebox using tetra-kis(dimethylamino)ethylene (TDAE, solvent N,N-dimethylform-amide, DMF).[16] Consistent with previous reports, NDI$^{-\bullet}$ absorbs throughout the visible region, with prominent band maxima at λ = 470, 600, 675 and 750 nm (Fig. S1, ESI†).[10] The anion radical is fluorescent with a broad envelope with well-defined vibronic structure and λ_{max} = 780 nm and emission quantum yield of 0.1% (Fig. S2, ESI†). It is noteworthy that there is a mirror-image relationship in the vibronic structure of the two lowest energy absorption peaks (675 and 750 nm) and the fluorescence spectrum, confirming that these features correspond to the transitions between the doublet ground state and the lowest doublet excited state. Time correlated single photon counting was applied to measure the fluorescence lifetime of NDI$^{-\bullet}$ and it was found to be τ = 250 ps (Fig. S2b, ESI†).

Picosecond TA spectra spanning the near-UV and visible regions for NDI$^{-\bullet}$ in DMF solution (c = 200 μM) were measured with 605 nm excitation, by analogy to previous reports of Wasi-lewski and co-workers,[29] and with 470 nm excitation, which corresponds to the maximum of the visible absorption spectrum of the NDI$^{-\bullet}$. The TA difference spectra are shown in two panels in Fig. S3 (ESI†). The time-resolved spectra are characterized by positive ΔA ranging from 325 to 450 nm and from 615 nm to 675 nm, corresponding to excited state absorption (ESA) of *NDI$^{\bullet-}$, and negative ΔA at λ_{max} = 470, 605 and 760 nm corres-ponding to ground state bleach (GSB) of the NDI$^{-\bullet}$ absorption bands (compare with Fig. S1, ESI†). The TA spectra of *NDI$^{-\bullet}$ are in good agreement with previous reports.[3,10] The lifetime of *NDI$^{-\bullet}$ was determined by single-exponential decay analysis of the ESA at 360 and 426 nm ($\tau \sim$ 200 and 195 ps, respectively), and the GSB at 474 nm ($\tau \sim$ 185 ps, Fig. S3c, ESI†). The lifetimes obtained by TA are in good agreement with the previous report by Wasilewski, who also used transient absorption and reported $\tau \sim$ 200 ps.[10] However, we note that the TA determined lifetimes are consistently $\sim$ 20% lower than was recovered by analysis of the fluorescence decay kinetics (τ = 250 ps), despite repeated measure-ments. In the quenching experiments described below, due to TA in UV region below 375 nm being obscured by ground state absorption of the quenchers, the ESA kinetics were monitored at 426 nm for Stern–Volmer analysis ($\tau^0 \sim$ 195 ps).

Stern–Volmer quenching experiments for *NDI$^{-\bullet}$ were carried out by using TA spectroscopy and by emission (lifetime) quench-ing. A series of 18 electron acceptors with reduction potentials varying from −0.86 V to −2.5 V were used as quenchers (see Table S1, ESI†). The quenching of the lifetime of *NDI$^{-\bullet}$ was monitored by TA using the ESA kinetics at 426 nm and by the emission decay at 770 nm. All the quenching data and Stern–Volmer plots are in the ESI† (see data in Fig. S5–S37). For acceptors with E_{red} > −2.2 V, quenching of the TA and fluorescence lifetimes were observed. By using the lifetime quenching data, Stern–Volmer plots were con-structed, and the bimolecular quenching rate constants, k_q, were determined by the relationship $k_q = K_{SV}/\tau^0$, where K_{SV} is the slope and τ^0 is the unquenched lifetime (195 ps for TA and 250 ps for fluorescence). The k_q values are listed in Table S1 (ESI†) for each acceptor, and Fig. 1 shows plots of the k_q values as a function of E_{red} for each quencher. From these plots can be seen that the k_q
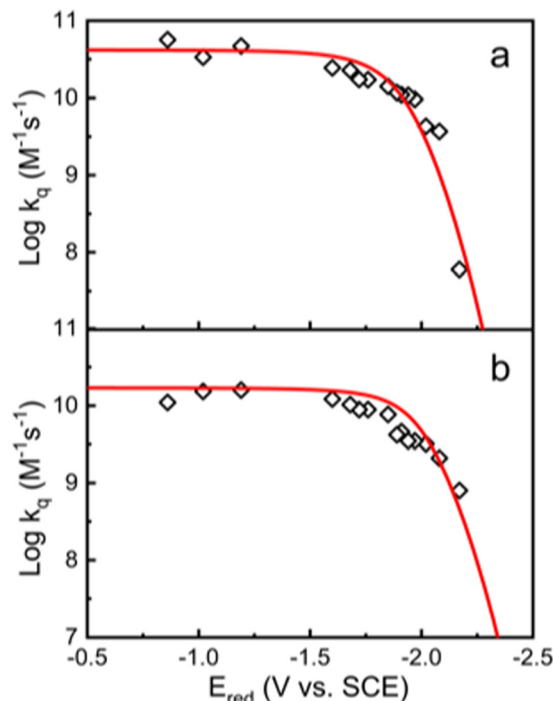

Fig. 1 Rehm–Weller plots for quenching of *NDI$^{-\bullet}$ by acceptors. Plots of quenching rates (k_q) vs. reduction potential of acceptor. (a) Quenching rates (k_q) determined by quenching of *NDI$^{-\bullet}$ excited state absorption monitored by transient absorption at 426 nm. Red line calculated using Rehm–Weller equation with E(*NDI$^{-\bullet}$/NDI) = −2.1 V. (b) Quenching rate determined by quenching of *NDI$^{-\bullet}$ fluorescence lifetime. Red line calculated using Rehm–Weller equation with E(*NDI$^{-\bullet}$/NDI) = −2.2 V. See ESI,† for details regarding the Rehm–Weller equation and calculation of lines. Note that ΔG_{FET} becomes more negative moving from right to left along the x-axis.

values are close to the diffusion limit ($\sim 1 \times 10^{10}$ M^{-1} s^{-1} in DMF) for acceptors with $E(A/A^-)$ > −1.5 V, and they fall off for acceptors with $E(A/A^-)$ < −1.5 V. The solid lines in Fig. 1a and b were calculated by using the Rehm–Weller equation (see ESI,† eqn (S1)). This expression correlates the rate of bimolecular ET with the driving force of forward ET, ΔG_{FET}, where $\Delta G_{FET} = E$(*NDI$^{-\bullet}$/NDI) $- E(A/A^{-\bullet})$. The fits of the data to the Rehm–Weller expression afford values for E(*NDI$^{-\bullet}$/NDI) = −2.1 V (for TA) and −2.2 V (for emission quenching). Notably, the values obtained from the Rehm–Weller plots are in excellent agreement with the value computed from the ground state reduction potential and the energy of *NDI$^{-\bullet}$, E(*NDI$^{-\bullet}$/NDI) = −0.56 − 1.59 eV = −2.15 eV (the energy of *NDI$^{-\bullet}$ is computed from its fluorescence maximum).

During the quenching study, the full time resolved TA spectra as a function of quencher identity and concentrations were measured, and these are all shown in the ESI.† Inspection of these data reveal a clear difference in the evolution of the TA spectra as the reduction potential of the acceptor varies. To highlight the difference, Fig. 2 compares the full set of TA difference spectra as a function of acceptor concentration for 3-nitrobenzaldehyde (3-NBA, E_{red} = −1.02 V) and ethyl-4-bromobenzoate (EBB, E_{red} = −1.97 V), and Fig. 3 shows the TA kinetics at wavelengths corresponding to the ESA and GSB
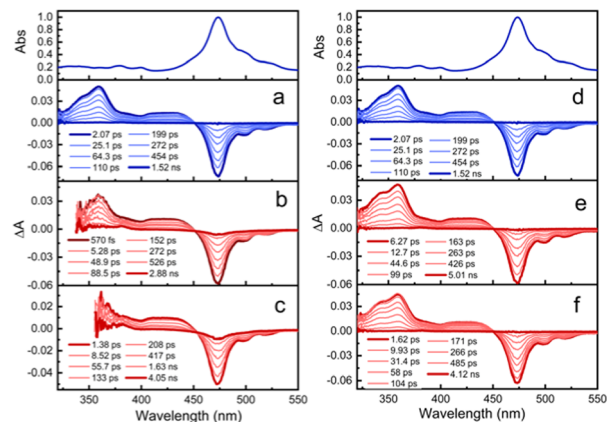
Fig. 2 Transient absorption spectra of 200 μM NDI$^{\bullet-}$ in the presence of 3-nitrobenzaldhyde (a) 0 M, (b) 0.05 M, (c) 0.1 M and ethyl-4-bromobenzoate (d) 0 M, (e) 0.2 M, (f) 0.4 M in DMF. UV-vis absorption of NDI$^{\bullet-}$ in DMF is included on top of the TA spectra for reference. Spectra are obscured at $\lambda < 375$ nm in (b) and (c) due to absorption of 3-nitrobenzaldehyde.

of NDI$^{-\bullet}$ (426 and 473 nm, respectively). The obvious difference is that for 3-NBA the GSB (473 nm) does not fully recover at long delay times (Fig. 2c and 3b), whereas for EBB the GSB recovers fully to $\Delta A = 0$ (Fig. 3d). The reason that the GSB of NDI$^{-\bullet}$ does not fully recover for 3-NBA quencher is that cage escape is occurring in this system (Scheme 1, step 3) which gives rise to the separated ET products neutral NDI and the reduced acceptor, 3-NBA$^{-\bullet}$. Convincing evidence that the neutral NDI is produced by cage escape is shown by the global analysis of the TA difference spectra for the NDI/3-NBA system (Fig. S23, ESI†), where it is seen that the long lifetime eigenspectrum clearly shows absorption features at 360 and 380 nm which correspond to neutral NDI. A similar global analysis of the NDI/4-nitrobenzaldehyde (4-NBA, Fig. S23, ESI†) system reveals peaks in the long time eigenspectrum at 360, 380 and 405 nm which are attributed to neutral NDI and the reduced acceptor, 4-NBA$^{-\bullet}$.[30] Inspection of the full set of quenching data in the SI reveals that as assessed by the recovery of NDI$^{-\bullet}$ GSB at long

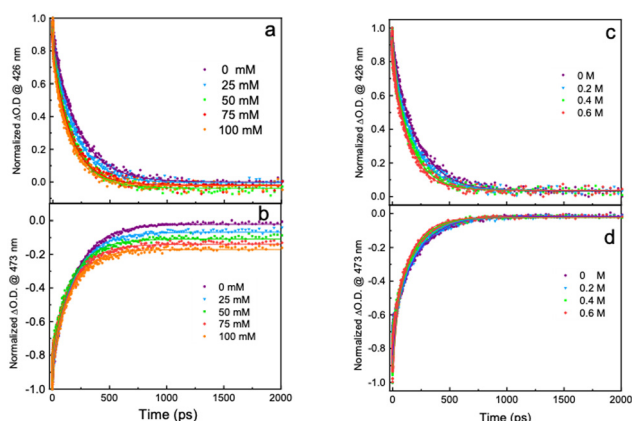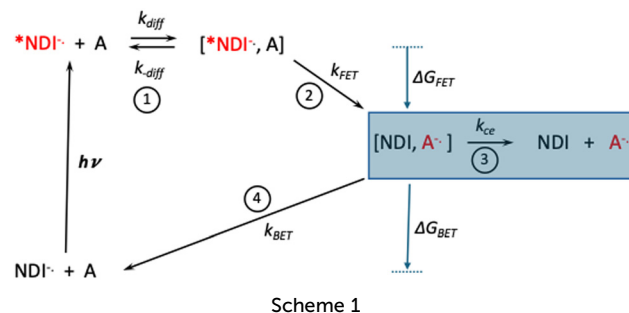**Fig. 3** Normalized transient absorption kinetic traces of 200 μM NDI$^{\bullet-}$ with 3-nitrobenzaldehyde (a) at 426 nm (b) at 473 nm and ethyl-4-bromobenzoate (c) at 426 nm (d) at 473 nm. Concentration of quenchers shown in insets.

Scheme 1

delay times, cage escape occurs for acceptors with $E_{red} > -1.2$ V, and for all the other acceptors ($E_{red} < -1.2$ V) the cage escape efficiency is low ($\eta_{ce} < 0.01$).

Scheme 1 illustrates the steps involved in the photoinduced reaction between *NDI$^{-\bullet}$ and the electron acceptors, with the rate constants defined for the individual steps.[27] Also indicated in Scheme 1 are the driving force for forward and back ET (ΔG_{FET} and ΔG_{BET}, respectively) which vary systematically with acceptor reduction potential (see below). In the context of photocatalysis, the efficiency of cage escape (step 3) to form the free reduced acceptor is as important as the efficiency of quenching by forward ET (step 2). This is because the lifetime of A$^{-\bullet}$ is increased significantly after cage escape, giving rise to the greatest probability of further reaction *via* uni- or bimolecular steps. Cage escape involves competition between back ET within the solvent cage product of ET (step 4) and separation of the ET products from the solvent cage (step 3) by diffusion apart. Quantitatively, the cage escape efficiency is given by the expression, $\eta_{ce} = k_{ce}/(k_{BET} + k_{ce})$, where the rate constants are defined in Scheme 1.[27] From this expression it can be deduced that η_{ce} increases as the rate of back ET (k_{BET}) decreases. Analysis of the cage escape efficiency data, coupled with calculated rates of cage escape ($k_{ce} \sim 6 \times 10^8$ s^{-1}, see ESI†) allows calculation of k$_{BET}$ for the three acceptors with $E_{red} > -1.2$ V. These data are summarized in Table 1. Quite interestingly, for these three acceptors, $\Delta G_{BET} > -0.6$ eV, which is in the Marcus normal region for ET.

Indeed, the observed rates for back ET are in accord with rates expected for ET between a moderately coupled donor–acceptor pair when the reactions are in the moderately exothermic, Marcus normal regime.[28,31] This is unusual for photoinduced ET reactions, where back ET is usually in the Marcus inverted region and is exceedingly rapid.[32] The reason that the back ET reactions are in the Marcus normal region is because the process involves a charge shift reaction between the

Table 1 Back electron transfer rates for selected acceptors[a]

Acceptor	$E(A/A^-)^b$/V	ΔG_{BET}^c/eV	$k_{BET}/10^9$ s^{-1}
Nitrobenzene	−1.19	−0.63	2.8
3-NBA	−1.02	−0.46	1.0
4-NBA	−0.86	−0.30	0.62

[a] See ESI for details regarding calculations. [b] SCE reference electrode, see Table S1 (ESI) for references. [c] Calculated by using $E(\text{NDI/NDI}^{-\bullet}) = -0.56$ V.

reduced acceptor and neutral NDI, and for acceptors with relatively low reduction potentials the reaction is weakly exothermic. For all of the other acceptors ($E_{red} < -1.2$ V), back ET is considerably more exothermic ($\Delta G_{BET} < -1.0$ eV) and occurs in the Marcus inverted region. We conclude that for these acceptors since $\eta_{ce} \sim 0$, $k_{BET} \geq 10^{11}$ s^{-1}.

In summary, we have demonstrated by using time resolved absorption and emission spectroscopy that the doublet excited state of the NDI anion radical is quenched by electron acceptors *via* a bimolecular, diffusion-controlled mechanism. No evidence was found for static quenching that would involve ground state complex formation between NDI$^{-\bullet}$ and the acceptors. Rehm–Weller analysis of the bimolecular quenching data reveal that *NDI$^{-\bullet}$ is a potent one-electron reductant, with $E_{ox} \sim -2.1$ V *vs.* SCE. Cage escape of the products of photoinduced ET occurs with good efficiency for acceptors with reduction potentials > -1.2 V due to relatively slow back ET in the solvent caged [NDI, A$^{-\bullet}$] pair. Taken together, the results support the notion that anion radical excited states can serve as potent one-electron donors *via* doublet excited states that can be accessed with low energy visible photons. The mechanistic study lends support to the conPET photocatalysis mechanism and gives insight into unusual thermodynamic consequences that arise from having photoreductants with such negative reduction potentials.

Data availability

The data supporting this article have been included as part of the ESI.†

Conflicts of interest

There are no conflicts to declare.

Notes and references

1 I. Ghosh, T. Ghosh, I. Bardagi Javier and B. König, *Science*, 2014, **346**, 725–728.
2 B. Pfund, D. Gejsnæs-Schaad, B. Lazarevski and O. S. Wenger, *Nat. Commun.*, 2024, **15**, 4738.
3 L. D. Mena, J. L. Borioni, S. Caby, P. Enders, M. A. Argüello Cordero, F. Fennel, R. Francke, S. Lochbrunner and J. I. Bardagi, *Chem. Commun.*, 2023, **59**, 9726–9729.
4 Y. Baek, A. Reinhold, L. Tian, P. D. Jeffrey, G. D. Scholes and R. R. Knowles, *J. Am. Chem. Soc.*, 2023, **145**, 12499–12508.
5 H. Kim, H. Kim, T. H. Lambert and S. Lin, *J. Am. Chem. Soc.*, 2020, **142**, 2087–2092.
6 N. G. W. Cowper, C. P. Chernowsky, O. P. Williams and Z. K. Wickens, *J. Am. Chem. Soc.*, 2020, **142**, 2093–2099.
7 F. Glaser, C. Kerzig and O. S. Wenger, *Angew. Chem., Int. Ed.*, 2020, **59**, 10266–10284.
8 S. Wu, J. Kaur, T. A. Karl, X. Tian and J. P. Barham, *Angew. Chem., Int. Ed.*, 2022, **61**, e202107811.
9 M. A. Fox, *Chem. Rev.*, 1979, **79**, 253–273.
10 D. Gosztola, M. P. Niemczyk, W. Svec, A. S. Lukas and M. R. Wasielewski, *J. Phys. Chem. A*, 2000, **104**, 6545–6551.
11 J. A. Christensen, J. Zhang, J. Zhou, J. N. Nelson and M. R. Wasielewski, *J. Phys. Chem. C*, 2018, **122**, 23364–23370.
12 N. T. La Porte, J. F. Martinez, S. Chaudhuri, S. Hedström, V. S. Batista and M. R. Wasielewski, *Coord. Chem. Rev.*, 2018, **361**, 98–119.
13 N. T. La Porte, J. A. Christensen, M. D. Krzyaniak, B. K. Rugg and M. R. Wasielewski, *J. Phys. Chem. B*, 2019, **123**, 7731–7739.
14 M. Fujita, A. Ishida, T. Majima and S. Takamuku, *J. Phys. Chem.*, 1996, **100**, 5382–5387.
15 S. Samori, M. Fujitsuka and T. Majima, *J. Phys. Chem. A*, 2008, **112**, 11312–11318.
16 C. Lu, M. Fujitsuka, A. Sugimoto and T. Majima, *J. Phys. Chem. C*, 2016, **120**, 12734–12741.
17 C. Lu, M. Fujitsuka and T. Majima, *J. Phys. Chem. C*, 2017, **121**, 649–655.
18 P. Brodard, A. Sarbach, J.-C. Gumy, T. Bally and E. Vauthey, *J. Phys. Chem. A*, 2001, **105**, 6594–6601.
19 J. Grilj, E. N. Laricheva, M. Olivucci and E. Vauthey, *Angew. Chem., Int. Ed.*, 2011, **50**, 4496–4498.
20 J. Grilj, P. Buchgraber and E. Vauthey, *J. Phys. Chem. A*, 2012, **116**, 7516–7522.
21 J. S. Beckwith, A. Aster and E. Vauthey, *Phys. Chem. Chem. Phys.*, 2022, **24**, 568–577.
22 A. R. Cook, L. A. Curtiss and J. R. Miller, *J. Am. Chem. Soc.*, 1997, **119**, 5729–5734.
23 M. Zamadar, A. R. Cook, A. Lewandowska-Andralojc, R. Holroyd, Y. Jiang, J. Bikalis and J. R. Miller, *J. Phys. Chem. A*, 2013, **117**, 8360–8367.
24 C. J. Zeman, S. Kim, F. Zhang and K. S. Schanze, *J. Am. Chem. Soc.*, 2020, **142**, 2204–2207.
25 D. Rehm and A. Weller, *Isr. J. Chem.*, 1970, **8**, 259–271.
26 C. Li, Z. Lin, Y. Li and Z. Wang, *Chem. Record*, 2016, **16**, 873–885.
27 M. J. Goodwin, J. C. Dickenson, A. Ripak, A. M. Deetz, J. S. McCarthy, G. J. Meyer and L. Troian-Gautier, *Chem. Rev.*, 2024, **124**, 7379–7464.
28 E. J. Piechota and G. J. Meyer, *J. Chem. Ed.*, 2019, **96**, 2450–2466.
29 N. T. La Porte, J. F. Martinez, S. Hedström, B. Rudshteyn, B. T. Phelan, C. M. Mauck, R. M. Young, V. S. Batista and M. R. Wasielewski, *Chem. Sci.*, 2017, **8**, 3821–3831.
30 T. Shida and S. Iwata, *J. Phys. Chem.*, 1971, **75**, 2591–2602.
31 C. R. Bock, J. A. Connor, A. R. Gutierrez, T. J. Meyer, D. G. Whitten, B. P. Sullivan and J. K. Nagle, *J. Am. Chem. Soc.*, 1979, **101**, 4815–4824.
32 M. R. Wasielewski, M. P. Niemczyk, W. A. Svec and E. B. Pewitt, *J. Am. Chem. Soc.*, 1985, **107**, 1080–1082.